Dependency of ice enhancement ratio on cloud top temperature in deep convective clouds: A numerical study

Deepak Waman

Department of Physical Geography and Ecosystem Sciences, Lund University

This document was compiled as a literature review to assess the current state of knowledge in the field of cloud microphysics. This study focuses upon the ice multiplication due to various secondary ice production mechanisms that may be active in natural clouds. The present work was conducted as a part of my PhD studies entitled "*Dependency of ice enhancement ratio on cloud top temperature in deep convective clouds: A numerical study*" and is supervised by Vaughan Phillips.

Contents

1. Introduction

Atmospheric cloud form when air in a rising air parcel becomes supersaturated with respect to liquid water (or ice in some cases). In many clouds, liquid and ice particles exist together. Ice particles in the atmosphere can be formed by heterogeneous freezing of cloud droplets in presence of suitable aerosol particles (known as ice nucleating particles [INPs]) at all temperatures below the freezing level and by homogeneous freezing of cloud droplets at temperatures colder than -36^{o}C in the upper troposphere. When present in clouds, ice particles can affect processes such as precipitation, cloud electrification and radiative transfer (Cantrell and Heymsfield, 2005; Field *et al*., 2017; Phillips *et al*., 2020).

The formation of ice particles is still one of the great challenges in the cloud physics. Below the freezing level the formation of ice is promoted in presence of IN. The first ("primary") ice formed from the activity of INP in clouds with tops warmer than -36^{o}C. Out of all aerosol particles (AP) in the atmosphere, very few of them can act as active INPs which makes them relatively rare in the atmosphere. The concentrations of active INP observed in the earth's atmosphere is in between 10^{-5} and 1 L^{-1} near -10^{o}C (Hobbs 1969; DeMott *et al*. 2003).

Although the concentration of active INP is relatively rare, it has always been observed that superabundant ice particles are found even when the cloud top is too warm for homogeneous freezing. Studies such as Hobbs *et al*. (1980) and Beard (1992) have shown that in natural clouds with tops warmer than about -15^{o}C the number concentrations of ice were up to a factor of 10^{4} higher than the available active INP concentrations. Therefore, it has long been proposed that following initial primary ice nucleation there must be some processes existing that are able to increase the number and mass concentration of ice. Such processes are known as secondary ice production (SIP). There is a range of SIP mechanisms that have been proposed in the past few decades. The Hallet-Mossop process is one of SIP mechanism and most widely accepted theory in which small ice splinters break away followed by riming of supercooled cloud droplets larger than 23 µm for temperature range -3 ^{0}C to -8 ^{0}C. Other SIP mechanisms are ice-ice collision (Vardiman 1978; Takahashi *et al*., 1995), droplet shattering (Leisner *et al*., 2014) and sublimation break-up (Bacon *et al*., 1998). In the mixed phase region (0 to -36^{o}C) SIP is the most important mechanism for controlling overall ice concentration (PK, 1997; Field *et al*. 2017). Although it is the most important mechanism of ice multiplication, SIP has received less

attention than heterogeneous ice nucleation. The accurate prediction of ice crystal concentrations is a major challenge for successful representation of microphysical properties of cloud as some recent cloud models can predict two moment size distribution (both mass and number ratio).

Precipitation can be in the form of rain, snow or hailstones and can occur when cloud particles reach to a certain critical size. There are two possible mechanisms responsible for formation of precipitation,

- *Cold rain process*- vapour growth of ice crystals (rime-splintering) (Rogers and Yau, 1996)
- *Warm rain process*- it involves formation of rain via coalescence in which small cloud droplets get captured by large drops to form raindrop.

Raindrops in *warm rain process* may become supercooled and it can form graupel followed by raindrop freezing (Phillips *et al*., 2001).

Over the decades, observations of size and concentration of ice particle have been measured using airborne optical array probe (OAP). It has been noticed that such airborne data is always dominated by small ice particles (< 100 μm) both in undersaturated and supersaturated environments (Korolev *et al*., 2011). However, modeling studies predicted that in environment that is supersaturated with respect to ice, small ice particles grow quickly to larger particles (e.g., snow, graupel or hail). Field *et al*. (2006)

1.1 Objectives

The study involves numerical modeling of clouds to study nucleation and multiplication of ice. Research objectives of this project are:

a. To simulate and validate the event of organized thunderstorms observed over Oklahoma, USA during the MC3E campaign in May 2011. To study dependency of various ice multiplication mechanisms (Phillips *et al*. 2017a, b; Phillips *et al*. 2018; Deshmukh *et al*. 2021) formulated in AC on cloud top temperature for the simulated MC3E case. To rank various SIP mechanisms based on their order of importance in convective clouds.

b. To develop new treatments of ice initiation based on laboratory observations of time-dependence freezing of natural INPs sampled by the Physics Department of Lund University (with project collaborator Thomas Kristensen) and incorporating latest published data about soot-IN into the AC's empirical parameterization of heterogeneous ice nucleation. To study the effect of time-dependent heterogeneous ice nucleation on overall ice nucleation by simulating ACAPEX (orographic case) and APPRAISE (supercooled, long-lived stratiform case).

c. Sensitivity tests with AC will reveal indirect effects from each IN species and their microphysical mechanisms (e.g., fragmentation of ice) for both cloud types listed above.

2. Basics of cloud microphysics

2.1 Nucleation

Nucleation involves change in phase. The possible phase changes are.

- Liquid-solid: freezing, melting
- Vapour-liquid: evaporation, condensation
- Vapour-solid: deposition, sublimation

Cloud droplets cannot form by homogeneous nucleation process as it requires higher supersaturations and such high supersaturations do not occur in the atmosphere. Droplet formation by heterogenous nucleation involves activation of APs.

2.1.1 Cloud condensation nuclei

Supersaturations with respect to water typically remain below 1% (PK, 1997). So, droplet formation in the atmosphere take place in presence of APs via heterogeneous nucleation in which water condenses onto existing APs. Such APs are known as cloud condensation nuclei (CCN). Soluble APs such as sea salt, ammonium sulfate can act as CCN and are able to initiate drops at different supersaturations below 1 %. The number concentration of CCN can be calculated using cloud chamber by measuring total number of drops activated per unit volume of air.

Due to less concentration of APs over ocean, CCN concentrations generally lower in maritime air masses (~ 10^2 cm^{-3}) while it is more (~ 10^3 cm^{-3}) over land (Radke and Hobbs, 1969; PK, 1997).

2.1.2 Droplet activation and Köhler theory

Activation is the process in which system goes from one stable state (low Gibbs free energy, [GE]) to another stable state (low GE), with an intermediate metastable state. Metastable state can be either supersaturated vapor or supercooled liquid. This transition requires to cross the energy barrier (maximum GE). Kelvin equation, which is as integral part of the Köhler theory, gives the analysis of this energy barrier.

Köhler curve consists of two terms:

i. Kelvin term or 'curvature effect'

Higher supersaturation with respect to the flat surface of pure water is needed to keep smaller droplets from evaporating. This is known as the curvature effect (Fig. 1, green curve) because the bonding between any two neighbouring water molecules on the curved surface of a droplet is comparatively weak than that on the flat surface of pure water. Hence, water molecules can escape from the curved surface of a droplet and enter in the vapour phase. Thus, high supersaturation is needed to keep the droplet growing. The greater the curvature, the greater the chance of water molecules on the surface to escape and evaporate.

Saturation vapor pressure is greater over the curved surface of a droplet than that over the flat surface. This is because the evaporation is greater over the curved surface of a droplet. Kelvin effect is important because all droplets grow from smaller (nanometer) to bigger (~ few μm) sizes. With increasing droplet radius, the equilibrium vapor pressure over a curved surface of a droplet becomes equal to equilibrium vapor pressure over a flat surface of pure water.

Homogeneous droplet nucleation is very unlikely in the atmosphere as the only way for this process to happen is continuous sticking of water molecules on the curved surface of a droplet. However, the radius of a nucleating drop is relatively small causing droplet to evaporate quickly. For droplet to form homogeneously and grow, supersaturation needs to be higher (RH > 200 %) which is not the case in the real atmosphere.

In case of heterogeneous nucleation, several water molecules can form coating outside of the aerosol particle. Droplet can continue to grow in typically lower supersaturation, at the expense of ambient vapor molecules.

ii. Raoult term or 'solute effect'.

The rate of evaporation of the solution (water with dissolved impurities such as CCN or INPs) is lower than that of the pure water. This is known as solute effect (Fig. 1, red curve) and it can partially compensate the Kelvin (curvature) effect. As the rate of evaporation is lower in the presence of impurities, the rate of condensation is more until there is an equilibrium between vapor flux to the surface (droplet) matches to that with the ambient flux. At equilibrium condition, saturation vapor pressure or equilibrium vapor pressure will be less than that required in the homogeneous nucleation. With increasing impurities, this equilibrium vapor pressure further decreases.

- If $RH_{dropet} > RH_{air}$, then rate of evaporation > rate of condensation. Droplet radius becomes small as water molecules leave the droplet. E.g., droplet C suffers evaporation causing droplet radii to drop to B.
- If $RH_{dropet} < RH_{air}$, then rate of evaporation < rate of condensation. Droplet radius increases due to net condensation.
- Droplet A also has $RH_{dropet} < RH_{air}$ and hence would tend to increase in size due to net condensation. However, in this part of the Köhler curve, increasing radii cause RH_{dropet}. This cause reduction in net condensation until the droplet radius reaches at B.

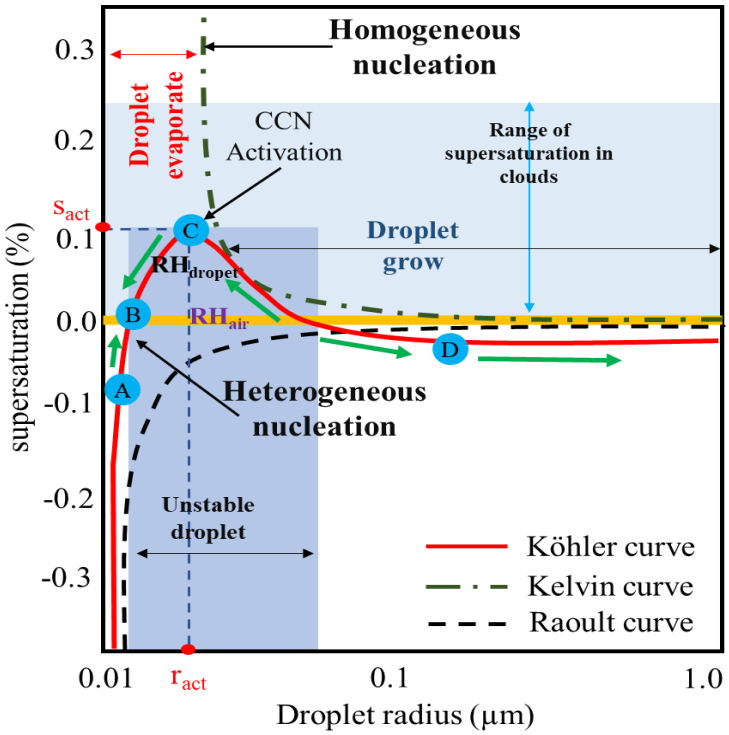

Fig. 1. Schematic representation of Köhler curve

2.1.3 Ice nucleating particles

Insoluble APs which are responsible for initiation of ice phase at temperatures warmer than -36^{o}C are known as ice nucleating particles (INP). There are basically four different modes by which ice nuclei can produce first ice in the cloud (PK, 1997),

- *Direct deposition*- When environment is supersaturated with respect to ice, water vapour at subzero temperatures can directly be absorbed by IN and it can later transform into ice.

- *Condensation freezing*- In this mode, an aerosol particle first acts as a cloud condensation nucleus (CCN) below 0^{o}C temperatures, forming a cloud drop which later freezes to form ice. This requires surrounding environment to be saturated with respect to water.

- *Immersion freezing*- this occurs at temperatures warmer than 0^{o}C in which an INP can immersed into a cloud drop. Once a drop temperature becomes sufficiently low, freezing is subsequently initiated.

- *Contact freezing*- In this mode, below freezing level ice phase is initiated by INP as soon as its contact happen with supercooled drop.

Some best examples of APs that can act as active INPs are dust, insoluble organic and primary biological aerosol particles (PBAP) such as fungi, bacteria, viruses, pollen, algae, detritus, etc (Patade *et al*. 2021).

2.2 Microphysical processes

Microphysical processes can be classified as warm and cold processes.

2.2.1 Warm microphysical processes

Clouds with its tops warmer than 0^{o}C are known as *warm clouds*. Warm clouds contain only water droplets. Microstructure of such clouds can be defined by properties such as droplet size, droplet diameter and liquid water content (Wallace and Hobbs, 2006).

Nucleation can only grow cloud droplet up to few micrometres in size so condensation alone cannot form precipitation. For precipitation to form in cloud, droplets must grow further by '*collision-coalescence*' process. Once formed by condensation, gravity cause droplets to fall with velocity called as terminal fall speed. Droplets that are larger in sizes will have a higher terminal fall speed. Such larger droplets will collide with smaller droplet lying in their paths while falling. Sometimes cloud droplets of different sizes stick together and coalesce to form a larger droplet. Such large cloud droplets then fall even faster and collide with smaller droplets in their path, aggregating more and more cloud droplets together, severing the positive feedback of collision-coalescence. The efficiency of collision-coalescence depends on the size distribution of cloud droplets. The wider the distribution of cloud droplet sizes, the more the chances of collision and coalescence. In general, typical cloud droplet ranges from 1µm to 100 µm and raindrop range from about 0.1 mm to 5 mm (drizzle drops at about 0.1 mm) in diameter.

2.2.2 Cold microphysical processes

Clouds whose tops reach to temperatures colder than 0^{o}C are referred as *cold clouds.* Such clouds may compose of liquid water, supercooled liquid water and ice or sometimes only ice. Clouds in which liquid and ice phase coexists are called as mixed phase clouds. Mixed phase of the cloud lies at temperatures between 0 and -36^{o}C. Below -36^{o}C level, homogeneous ice nucleation is predominant and cloud is said to be ice phase. In clouds with tops extending up to the tropopause all these phases coexist. Precipitation in cold clouds can form by *cold rain process* (Sect. 1) in which ice crystal formed during nucleation (Sect. 2.1.2) will first grow by diffusion of water vapour in presence of active INP (at temperatures warmer than -36^{o}C) and further growth may result into snow formation followed by riming or aggregation. Snow may rime to form graupel. Graupel may later melt while falling out. Heavily rimed ice crystals can result in hail formation.

2.3 Growth of ice crystal

Once the first ice crystal is formed in cloud (Sect. 2.1.2), it can further grow by diffusion, accretion, or aggregation. Growth of ice crystals depends on the temperatures and saturation level in the cloud.

2.3.1 Growth processes

i. Growth by diffusion

Nucleation generates the first ice crystals in a mixed phase cloud. Mixed phase cloud is dominated by supercooled cloud droplets and the air is saturated with respect to liquid water and therefore it is supersaturated with respect to ice. Hence a vapour pressure gradient develops between supercooled droplets and crystals and water vapour movement takes place from droplets to crystals. In such environment ice crystals will grow from vapour phase. Eventually, ambient air becomes sub-saturated with respect to water and to maintain the equilibrium the droplets evaporate. Droplet evaporation creates excess water vapour and hence ice crystals will grow further making cloud glaciated.

ii. Growth by riming and aggregation

Diffusion process generates 'cloud-ice' crystals that are smaller than 300 μm. Such crystals can grow to large ice crystals such as snow (300 μm to few centimetres) through process called '*accretion*' which involve collision of ice crystals with supercooled droplets.

In a mixed phase cloud, if ice crystals collect supercooled liquid droplets which stick on contact and freeze, the process is known as growth by *riming*. Riming can form various rimed structures for example, rimed column, rimed plate, spherical graupel, rimed needle, etc. Extreme riming forms graupel (0.3 to 5 mm) and in some cases hail (> 5 mm) which are dense particles of ice precipitation. Vigorous convective clouds (e.g., thunderstorm) forms hailstones due to their high liquid water contents.

Like cloud droplets, ice particles with different terminal fall velocities can collide while falling in the cloud. *Aggregation* is the third mechanism of ice crystals growth which involves ice crystals to collide and stick (aggregate) together. Aggregation depends on temperature and crystal type. Colliding ice crystals can become more adhesive when their surfaces become sticky, and this happen when temperature increases to above -5^{o}C (Houze, 1977). Ice crystals

with branches can get mechanically interlocked forming bigger aggregates such as snow (> 0.3 mm in diameters) (PK, 1997).

2.3.2 Secondary ice production and ice enhancement

It is always observed that the ice crystal concentrations in natural clouds is always high by some orders of magnitude than the available active INP (Sect. 1). Processes producing this excess ice concentration are known as SIP. Many field campaigns involving either aircraft measurements (Hobbs *et al*. 1974b) or handheld instruments have shown SIP to be active. Observations such as those by Auer *et al*. (1969) in stable orographic cap clouds over Wyoming, over Cascade mountains in the USA (Hobbs, 1969; Hobbs *et al*. 1974b) and by Mossop and Ono (1969) in cumulus clouds over Australia and Tasmania have supported the existence of SIP mechanisms that are responsible for ice multiplication. For accurate prediction of ice concentration in natural clouds it is important to account SIP processes. There is a range of ice multiplication mechanisms by which secondary ice can be formed such as the HM process of rime splintering, fragmentation in ice-ice collisions, fragmentation during raindrop freezing, and sublimation breakup.

1. The Hallett-Mossop process of rime-splintering

The Hallett-Mossop (1974, hereafter 'HM') process formation of small ice splinters that breaks away during the riming of supercooled cloud droplets that are typically larger than 24 μm in diameter and have an impaction speed of at least 0.2 m s^{-1} at temperatures between -3 and -8^{o}C. Several laboratory studies (Hallett and Mossop, 1974; Mossop and Hallett, 1974; Mossop, 1976) observed that under suitable conditions, per 100 to 250 cloud droplets (> 24 μm) impacting on the riming ice surface, 1 secondary ice splinter is produced. The production rate of the HM process is maximum at -5^{o}C.

2. Fragmentation in ice-ice collisions

Secondary ice may produce when two or more ice particles collide on each other. Laboratory and field studies such as those by Vardiman (1978), Takahashi *et al* (1995; reviewed by Phillips *et al*. 2017a, b) have observed production of secondary ice splinters in collisions of two or more ice particles. Hobbs and Farber (1972) based on theoretical consideration and field observation concluded that fragmentation due to graupel and dendrites is a likely mechanism for ice enhancement. Fragmentation in ice-ice collisions have reported by several modeling studies

such as those by Fridlind *et al* (2007) (crystal-crystal collision), Yano and Phillips (2011) (fragmentation in graupel-graupel collision) and Phillips *et al* (2017a) (fragmentation in collisions involving crystal, snow and graupel).

3. Fragmentation during raindrop freezing

Laboratory studies such as those by Johnson and Hallett (1968), Pruppacher and Schlamp (1975) and Leisner *et al* (2014) observed fragmentation of freezing raindrops or drizzles. While raindrop is freezing, liquid water may get trapped inside of an ice shell and pressure is continuing to build on it. The external ice shell breaks when this pressure exceeds a threshold during successive freezing of a drop and fragments and spikes get emitted. This can happen many times during the freezing of a given drop (King and Fletcher, 1973). Two possible modes of raindrop freezing fragmentation is proposed by Phillips *et al* (2018):

- Mode 1- Fragmentation during freezing of supercooled raindrop on collision with a less massive ice particle.
- Mode 2- Fragmentation during collision between a supercooled raindrop and a more massive ice particle.

4. Sublimation breakup

Secondary ice may also produce by fragmentation of ice particles during sublimation. Laboratory studies such as those by Schaefer and Cheng (1971), Oraltay and Hallett (1989), Dong *et al* (1994) and Bacon *et al* (1998) observed such breakup of ice. Oraltay and Hallett (1989) observed ice fragmentation in dendritic crystals sublimation. Based on these experiments Deshmukh *et al* (2021, now in press) formulated fragmentation of ice during sublimation breakup of rimed particles such as graupel and dendritic crystals.

3. Experimental setup for simulation of convective storm

3.1 Case description

The case is a line of convective clouds observed in north-central Oklahoma during Midlatitude Continental Convective Cloud Experiment (MC3E) on 11 May 2011 (Jensen *et al*., 2016). The clouds had warm bases near 17 ^{0}C at about 1.5 km altitude above mean sea level. The ground was elevated at an altitude of about 350 m MSL. The line of Mesoscale Convective System (MCS) consists of many cloud types, most of which were deep convective (e.g., cumulonimbus) with typical cloud depth of 9-13 km and stratiform clouds. The case had a very large amount of CAPE near the beginning of the period where lower atmosphere was entering a moistening trend but still had a mid-level humidity deficit (Jensen *et al*., 2016). MC3E included observations of cloud microphysics by the NASA ER-2 aircraft functioned at the top of the sampling domain (~ 20 km in altitude above MSL). It carried High-Altitude Imaging Wind and Rain Airborne Profiler (HIWRAP), two multifrequency passive microwave radiometer: Advanced Microwave Precipitation Radiometer (AMPR) and Conical Scanning Microwave Imaging Radiometer (CoSMIR) (Jensen *et al*., 2016). The University of North Dakota (UND) Cessna Citation II jet aircraft served as the in-situ microphysics platform with a primary emphasis placed on the measurements of ice-phase hydrometeors at altitudes between the melting level and cloud top (~ 4 - 13 km). The Citation carried a standard suite of meteorological instruments together with cloud and precipitation microphysical probes and total and liquid water content probes (Jensen *et al*., 2016).

3.1.1 Airborne and ground-based measurements

At the top of the study domain, NASA ER-2 aircraft carried High-Altitude Wind and Rain Airborne Profiler (HIWRAP), Advanced Microwave Precipitation (AMPR), the Conical Scanning Microwave Imaging (CoSMIR) multifrequency radiometers and dual frequency, dual beam (30^{o} and 40^{o} incidence angles) nadir pointing Doppler radar (Jensen *et al*., 2016). The University of North Dakota (UND) Cessna citation II aircraft carried a suit of meteorological instruments, viz., cloud microphysical, liquid and water content and precipitation probes. These probes made measurements of in-cloud microphysical properties such as ice number

concentrations, drop size and concentration, liquid water content (LWC), etc at altitudes between melting level and cloud top. Combine Spectrum uses particle size distribution of CIP (or 2DC) merged with HVPS3. All instruments mounted on citation aircraft are listed in table 1.

Measurements of aerosols, meteorological conditions such as temperature, wind, surface precipitation etc., was conducted by the dedicated suite of instruments deployed at the ARM SGP CF. Surface precipitation was measured with pairs of 16 rain gauge within 6 km radius of the SGP central facility. Measurement of the spatial variability of momentum, surface heat fluxes and moisture across the SGP region was done with 20 extended facilities covering an area of 150 km x 150 km.

Table 1. Instruments mounted on citation aircraft during MC3E

Instrument	Range
2D cloud imaging probe (2D-C)	0.03-1.0 mm
Cloud imaging probe (CIP)	0.025-1.5 mm
King hot-wire liquid water content (LWC) probe	0.1-5 g m^{-3}
Cloud droplet probe (CDP)	2-50 µm
Nevzorov probe	0.03-3 g m^{-3}
High-volume precipitation spectrometer, version 3 (HVPS-3)	0.15-19.2 mm

The MC3E case simulated (11 May 2011) with the AC consisted of stratiform and mostly deep convective (e.g., cumulonimbus) with typical cloud depth of 9-13 km. The clouds had relatively warm bases (17^{o} C) at about 1.5 km altitude above mean sea level. The ground was elevated at an altitude of about 350 m MSL.

3.2 Description of numerical cloud model

In this study, Aerosol-Cloud model (AC) is used. The AC has a representation of clouds and aerosols with a hybrid spectral bin-two-moment bulk microphysics, semiprognostic aerosol and interactive radiation and schemes (Phillips et. al., 2017; 2020). The grid spacing of AC is

2 km horizontally and about 0.5 km vertically, with time step of 10 s. The domain is 3D mesoscale and about 80 km wide. The lateral boundary conditions are periodic in both the east-west and north-south sides of the domain.

Tagging tracers (passive prognostic variables) were used to track and estimate the number and mass concentration of ice formed in each process (i.e., primary, secondary ice and ice from homogeneous freezing). These variables do not interact with any other process in the AC model.

From the initial sounding and aerosol profiles, AC predicts the in-cloud size distributions of aerosol and in-cloud supersaturation. Figure 2 shows the initial sounding of AC. Hourly sounding profiles of ambient temperature, mixing ratio, wind is created. These are then input to the microphysics scheme to predict numbers of cloud droplets and crystals nucleated (Phillips et. al., 2017b). Seven aerosol species governed primary initiation of hydrometeors, with heterogeneous and homogeneous nucleation of ice. AC represents microphysical species in four categories viz., rain, cloud ice ("crystals"), snow and graupel/hail. Four types of fragmentation are treated to form secondary ice:

1. Hallet and Mossop (1974) rime splintering (cloud droplets > 24 μm in diameter),
2. fragmentation in ice-ice collisions (Phillips *et al*., 2017a, b),
3. shattering of freezing rain/drizzle (Phillips *et al*., 2018),
4. sublimation breakup of snow and graupel (Deshmukh *et al*., 2021).

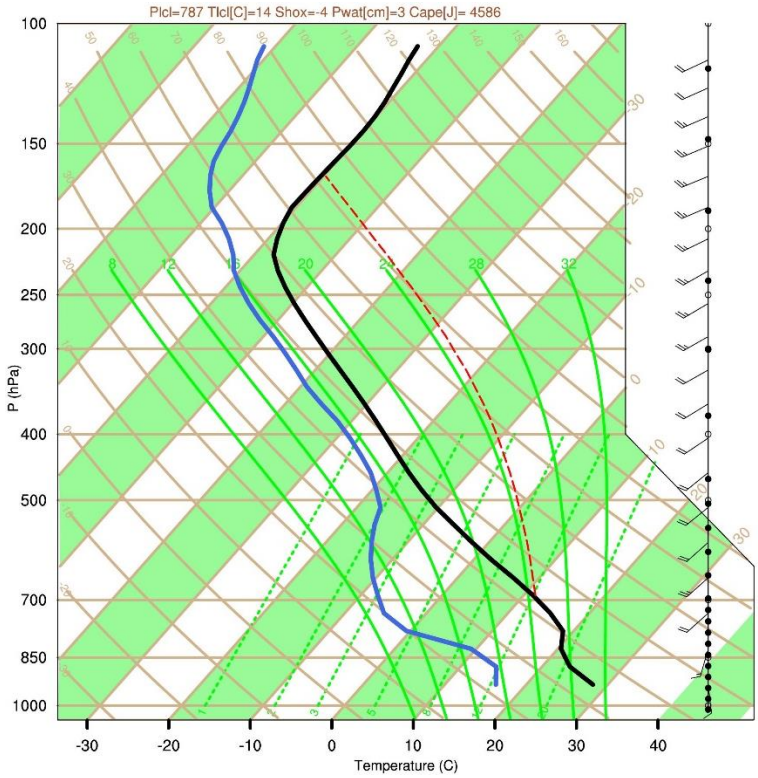

FIG. 2. Initial vertical profile of dewpoint (blue line) and environment temperature (black line) on 10 May 2011 at 00:00 UTC. The thin dotted red line shows the moist adiabat.

Aerosol loadings were derived from Interagency Monitoring of Protected Visual Environments (IMPROVE) network deployed at stations nearby as MC3E campaign made no measurements of aerosols. However, the measurement of the number concentration of condensation nuclei were made by the condensation particle counter (CPC; TSI-3771) which was mounted on the University of North Dakota (UND) Cessna Citation II jet aircraft. The CPC measures the particle concentrations of aerosols between 10 nm to 1μm in diameter. Figure 3 shows that the predicted aerosol concentration agrees well with the CPC observation in the mid-tropospheric region. A threshold value of cloud droplet concentration of 5 cm^{-3} from the cloud droplet probe was used to filter the raw CPC data.

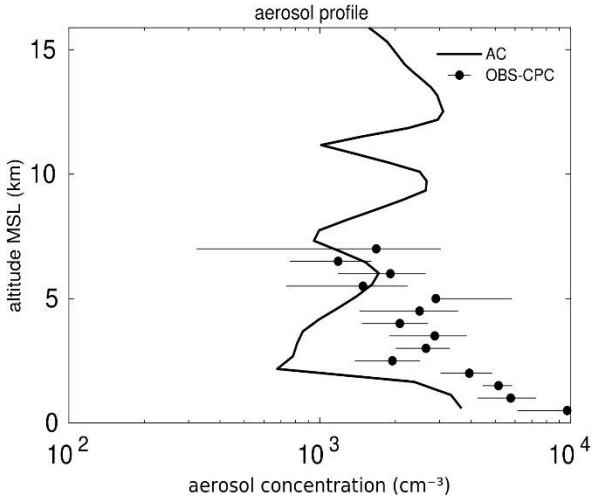

FIG. 3. The predicted profile of aerosol concentration for the MC3E case (11 May 2011) at the model initialization for the environment at about 350 m MSL altitude. This is compared with the observation from CPC mounted on citation aircraft.

Initial concentrations of seven aerosol species of AC were derived from the Goddard Chemistry Aerosol Radiation and Transport (GOCART) model (Chin *et al*., 2000). Aerosol mass concentration profiles were scaled at all levels to match simultaneous measurements by IMPROVE averaged from Wichita Mountains (600 m mean sea level (MSL)), Ellis (640 m MSL), and Stilwell (330 m MSL) sites in Oklahoma, USA. Observed concentrations were 0.06 μg m^{-3} for sea salt, 0.7 μg m^{-3} for sulphate, 0.345 μg m^{-3} for insoluble organic and 1.38 μg m^{-3} for soluble organic, 0.25 μg m^{-3} for black carbon, 0.175 μg m^{-3} for dust. Also, AC has representation for several groups of primary biological aerosol particles (Patade *et al*., 2021) and observed concentrations were 0.053 μg m^{-3} for pollen, 0.067 μg m^{-3} for fungi, 0.023 μg m^{-3} for bacteria, 0.029 μg m^{-3} and 0.000043 μg m^{-3} for detritus and algae, respectively.

Figure 4a shows predicted activity spectrum of cloud condensation nuclei (CCN) from size distribution of soluble aerosols at model initialization which is similar to the CCN activity observed at the Southern Great Plains (SGP) site for a similar altitude (300 m MSL). Figure 3b shows the number concentration of predicted active INP compared with continuous flow diffusion chamber (CFDC) observation made by DeMott *et al*. (2015) during spring 2014 at the SGP. The Different year dataset is used here to compare the model predicted active INP concentrations as MC3E campaign made no measurements of active INPs. To be consistent with the timeframe of the MC3E campaign, the data from DeMott *et al*. (2015) was reprocessed for corrections and averaged for May 2014.

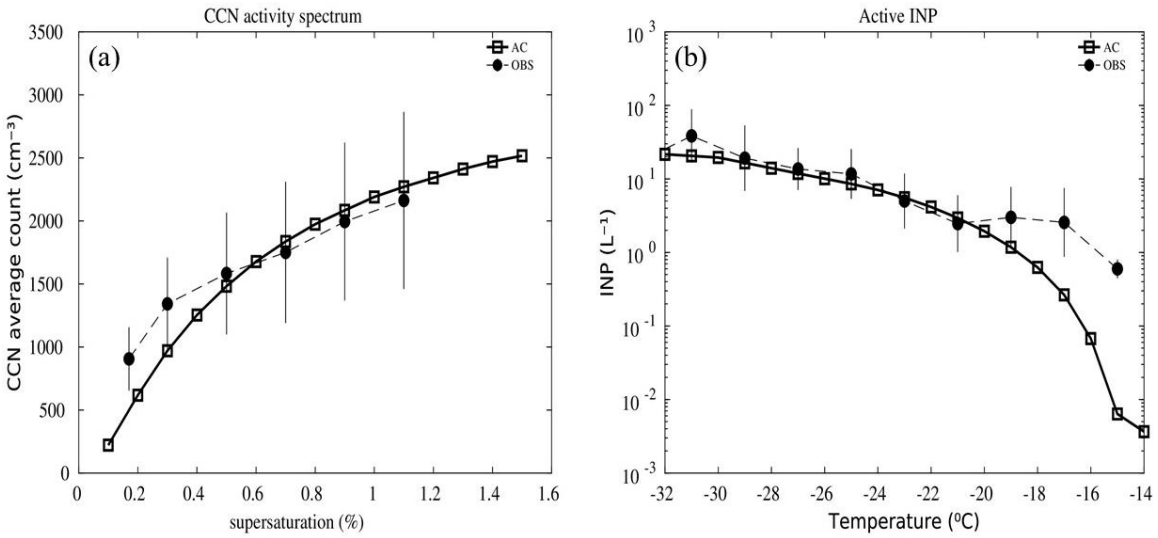

FIG. 4. The predicted activity spectrum of (a) CCN corresponding to the prescribed vertical profiles of size distributions of various aerosol species (solid line). CCN activity of AC is compared with the corresponding 3-day (9-12 May) averaged activity from the CCN counter (CCN-100) deployed at Lamont, Oklahoma. (b) Predicted active INP activity (solid line) compared with CFDC observation (dotted line) taken at the SGP site in 2014 (adapted from DeMott *et al*., 2015, with changes). Both the profiles are at the model initialization.

4. Objective 1

4.1 Cloud-top detection

The cloud top temperature for the simulated MC3E case (Sect. 3.1) is detected using cloud-top detection algorithm. It is described as follows:

First, the convective cores are automatically identified using the partitioning method (Xu, 1994). According to this method, a convective core satisfies one of the following three conditions:

i) The horizontal distribution of maximum cloud draft strength ($|w_{max}|$) is twice as large as the average over the adjacent four grid columns, or,

ii) $|w_{max}|$ is greater than 3 m s^{-1}, or,

iii) Surface precipitation rate ($<P>$) is greater than 25 mm h^{-1}.

Grid columns for which the total liquid water path (TLWP) is positive and other than the convective core was selected as convective grid columns. Following Tao and Simpson (1989), a convective region is defined as a region including a core and immediately adjacent convective grid columns. The grid columns other than these and for which TLWP exceeds 0.2 kg m^{-2} were defined as stratiform regions and the remaining grid columns were identified as clear regions.

After identifying the convective regions, following steps were followed to form a complete cloud structure:

1. Instantaneous grid point grouping

Once a core and its adjacent convective columns (convective region) was identified, links were established between pairs of adjacent convective grid points at any given time. Each convective region was expanded further using these links. Such links of grid points were then stored as individual instantaneous cloud group.

For example, in Fig. 5, group 2 consist of a core (i+1, j) and creates the first link with adjacent grid point (i+2, j+5) and the second link with grid point (i+1, j+6).

2. Iterative grouping

Now a problem is that as cloud evolve with time in the simulation, a convective region may split in multiple convective regions. Such splitting later forms so called "*extra clouds*". These extra splitting were identified by defining '*spatial-temporal links*' between pairs of convective grid points ($|w| > 1$ m s^{-1}) that are adjacent in spatial-temporal sense (in 4D). Such *clusters* of contiguous spatial-temporal links in space-time were grouped together.

3. True cloud groups

These expanded convective regions (step 3) may have overlapped even though they are different clouds in the simulation. That means there could be multiple clouds for a given convective region formed in step 1 and 2. All convective regions were then partitioned into distinct "*sub-cloudy regions*". To avoid overlapping amongst convective regions (step 2), two sub-groups of convective regions were defined for a given instance of time. If the grid points of these two sub-groups of a convective region were different, then there was no overlap. And if the grid points were the same, then they said to be overlapped. These no-overlapped "*sub-cloudy regions*" then saved in "*true cloud groups*".

4. Grouping true cloud groups: Actual cloud

Once *true cloud* grid points associated for a given core were found, convective columns in such a core were collected along with the convective grids adjacent to these columns, and an actual cloud was formed as shown in Fig. 11.

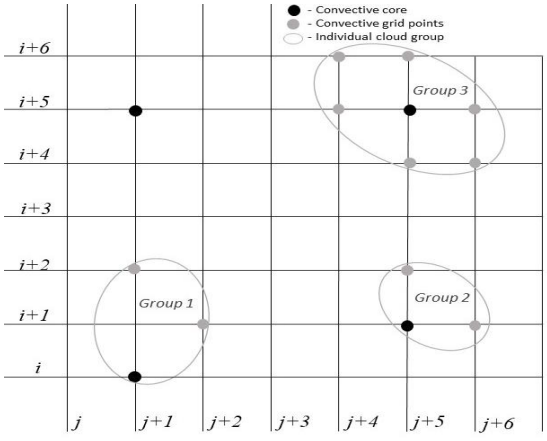

Fig. 5. Schematic diagram representing instantaneous cloud grouping in the control simulation of AC. Filled grey circles represents convective grids and filled black circles represents cores.

4.2 Results

4.2.1 Model validation

The convective line observed (Sect. 3.1) in MC3E on 11 May 2011 has been simulated by AC (Sect. 3.2). Various predicted microphysical properties such as cloud droplet diameter, number concentrations of droplet and ice particles, liquid water content, etc. and surface precipitation, radar reflectivity are validated against aircraft and ground-based observations. Convective updrafts and downdrafts regions were identified by selecting vertical velocities (w) greater than 3 m s^{-1} and less than – 3 m s^{-1} respectively, in the model and aircraft data. The estimated error in vertical velocity observed by aircraft is about 30 %.

Figure 6a, b shows predicted domain averaged precipitation rate and accumulated precipitation, respectively. Because of the classic overshoot for the onset of convection in the model, the predicted precipitation rate is higher (by about 60 %) than the radar observed rate in the first peak (10 May, 24 UTC). However, the predicted rate of precipitation is less than the observed rate by 40 % in the second peak of the simulation (11 May, 19 UTC). For the initial periods (10 May, 12-24 UTC) of the simulation, the predicted CAPE is significantly high (3500 J kg^{-1}, Fig. 6c) producing higher precipitation in the first peak. However, the second peak of the simulation (11 May, 15-21 UTC) is characterized by relatively less CAPE (1700 J kg^{-1}) which brought less precipitation in the second peak.

The predicted characteristics of cloud droplets such as mean droplet diameter (Fig. 6d, e), droplet concentrations (Fig. 6f, g) and liquid water content (Fig. 6j, k) were similar to the aircraft observations for both convective cloudy updrafts and downdrafts. The predicted distribution of updraft speeds (> 3 m s^{-1}) are in good agreement with aircraft observation and differ no more than 50 % (Fig. 6o). The predicted radar reflectivity agrees with the KAZR observations (Fig. 6p). Domain averaged predicted shortwave (Fig. 6q) and longwave (Fig. 6r)

radiative fluxes measured at the top of the atmosphere (~ 100 hPa) agrees with the satellite (GOES VISST) observations with errors at any given time of less than 30 %.

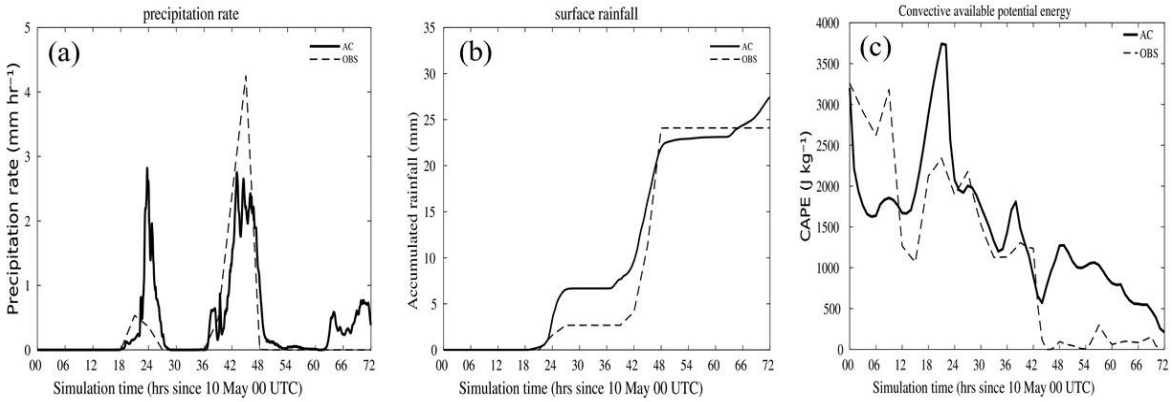

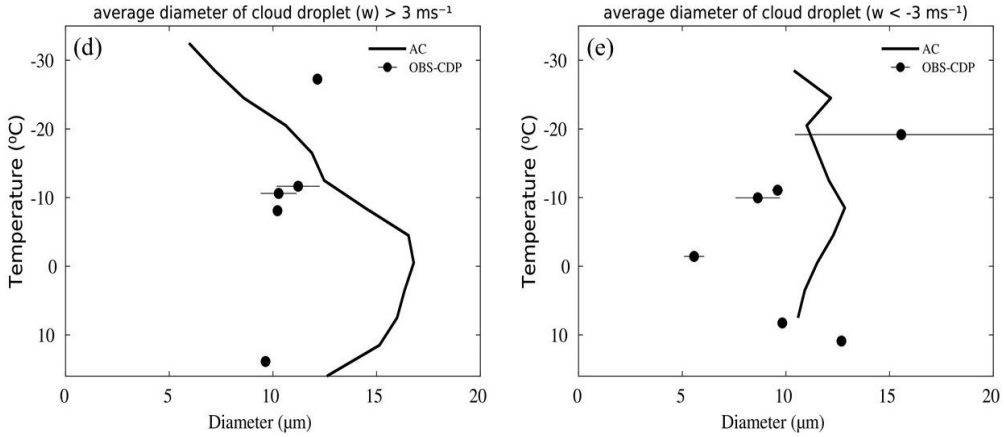

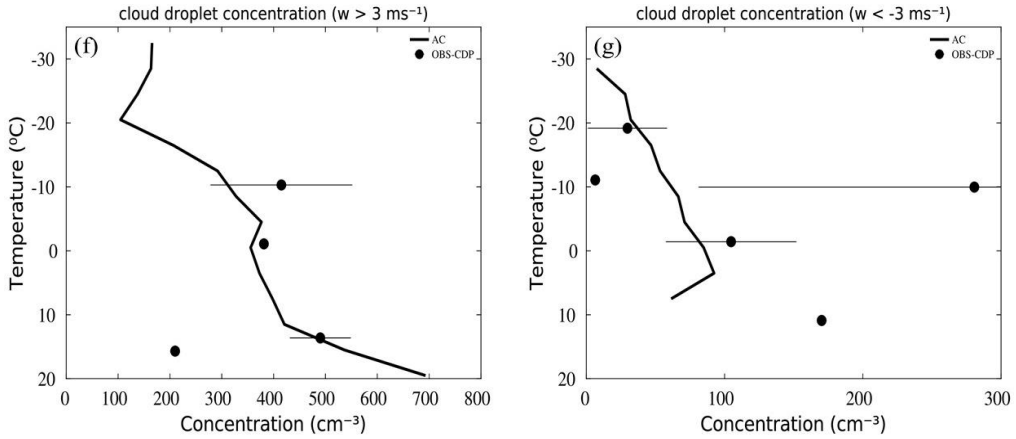

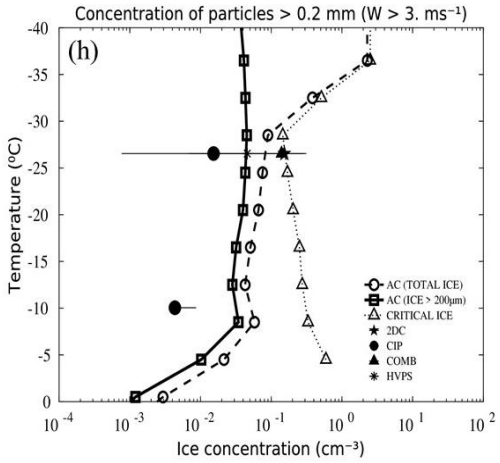
Concentration of particles > 0.2 mm (W > 3. ms⁻¹)
(h)
Temperature (°C)
Ice concentration (cm⁻³)
AC (TOTAL ICE)
AC (ICE > 200μm)
CRITICAL ICE
2DC
CIP
COMB
HVPS

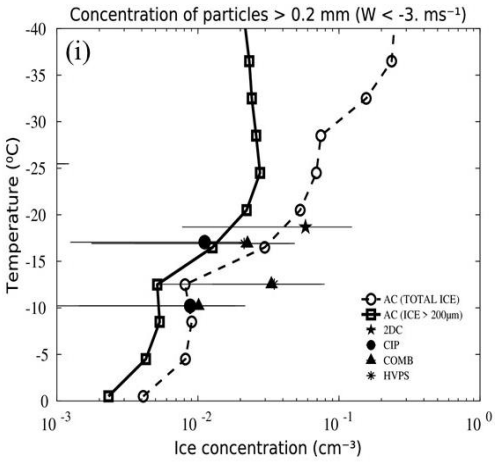
Concentration of particles > 0.2 mm (W < -3. ms⁻¹)
(i)
Temperature (°C)
Ice concentration (cm⁻³)
AC (TOTAL ICE)
AC (ICE > 200μm)
2DC
CIP
COMB
HVPS

569

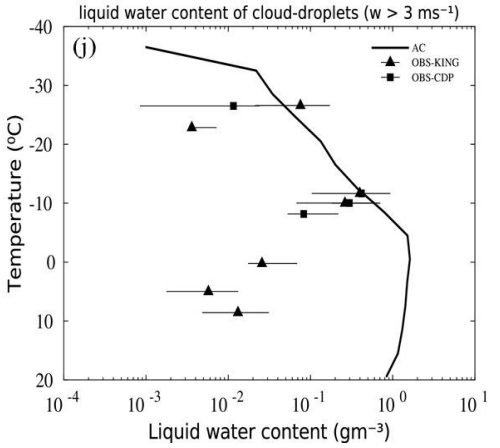
liquid water content of cloud-droplets (w > 3 ms⁻¹)
(j)
Temperature (°C)
Liquid water content (gm⁻³)
AC
OBS-KING
OBS-CDP

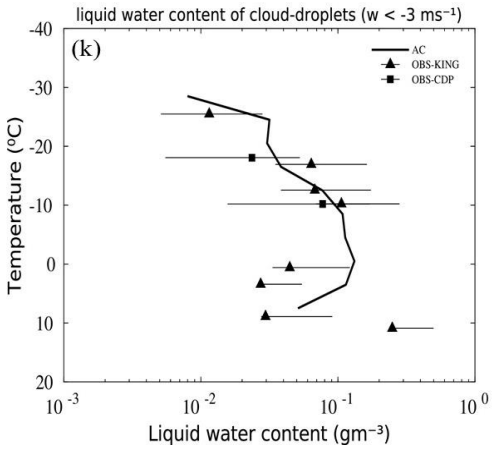
liquid water content of cloud-droplets (w < -3 ms⁻¹)
(k)
Temperature (°C)
Liquid water content (gm⁻³)
AC
OBS-KING
OBS-CDP

570

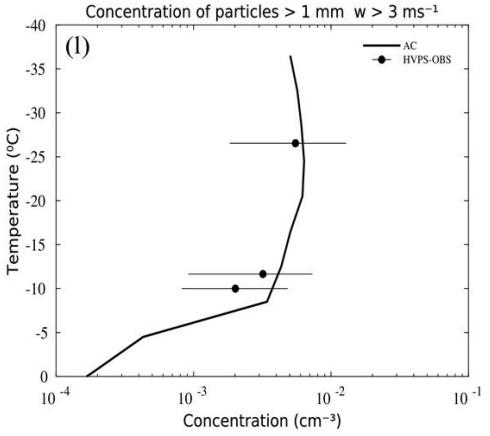
Concentration of particles > 1 mm w > 3 ms⁻¹
(l)
Temperature (°C)
Concentration (cm⁻³)
AC
HVPS-OBS

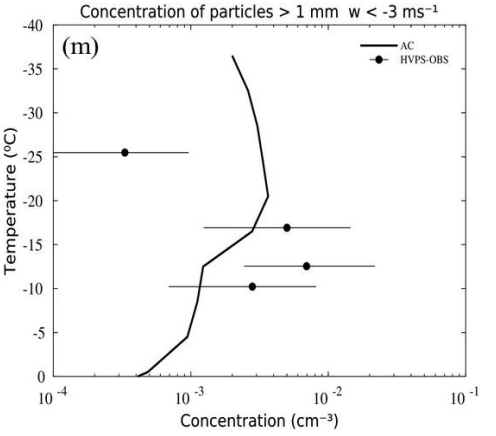
Concentration of particles > 1 mm w < -3 ms⁻¹
(m)
Temperature (°C)
Concentration (cm⁻³)
AC
HVPS-OBS

571

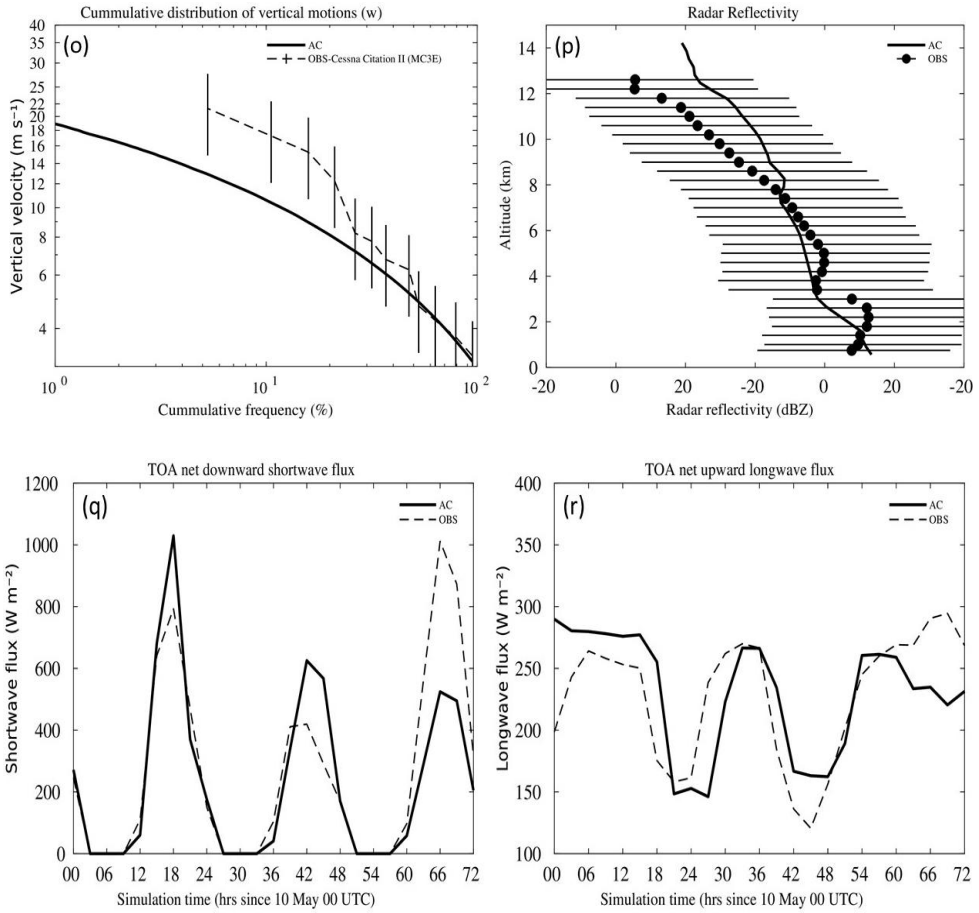

Fig. 6. Comparison of control simulation by AC (full line) of the MC3E case with radar, satellite, and aircraft observations (dotted line) for the period of 10 May 00 UTC-13 May 00 UTC. (a) predicted precipitation rate (mm hr^{-1}) at surface compared with observations from rain gauge adjusted WSR-88D radar over the SGP site. (b) predicted precipitation accumulation (mm) at surface compared with observations same as in (a), (c) predicted convective available potential energy (CAPE) compared with observed sounding. (d, e) mean cloud droplet size conditionally averaged over convective cloudy updraft ($w > 3$ m s^{-1}) and downdraft ($w < -3$ m s^{-1}) conditions compared with aircraft observations from the CDP probe, (f, g) cloud droplet concentrations at these vertical velocities compared with aircraft observations from the CDP probe, (h, i) filtered (> 200 μm) ice particle (cloud-ice, snow, and graupel) concentrations over cloudy convective updrafts and downdrafts conditions both predicted and observed by CIP, 2DC, HVPS3 and COMB-SPECTRUM probes on the aircraft. Theoretical critical ice concentration calculated from Korolev and Mazin (2003, formula 22 therein) is shown with dotted line. (j, k) predicted liquid water content over faster convective cloudy updrafts (> 3 m s^{-1}) and downdrafts (< -3 m s^{-1}) compared with observations from KINGS hot wire and CDP probes mounted on the aircraft, (l, m) Predicted ice particle concentrations (> 1mm, rain+snow+graupel) compared with HVPS3 probe in such faster updrafts and downdrafts. (o) Histogram of vertical velocity in fast convective updrafts (> 3 m s^{-1}) compared with observations from citation aircraft, (p) Conditionally averaged (> -20 dBZ) predicted radar reflectivity vertical profile compared with ground-based radar (KAZR), (q, r) predicted top of the atmosphere (TOA) radiative fluxes of shortwave and longwave radiation compared with satellite (GOES VISST) data. Errorbars shown in corresponding plots are standard errors of observational samples.

2DC and HVPS3 had 'shattering corrected' tips while CIP was without any such 'anti-shatter' tips. Data from such probes which had no 'anti-shatter' tips were later corrected based on

method described in Field *et al*. (2006) and only ice particles with maximum size dimension greater than 200 μm were included in the plotted ice concentration (Fig. 6h, i) both in observation and simulation. The predicted filtered ice particle concentrations are on the order of 10 L^{-1} at observational levels and the same order of magnitude can be seen in the aircraft data for cloudy convective updrafts ($w > 3$ m s^{-1}) and downdrafts ($w < -3$ m s^{-1}) (Fig. 6h, i). In downdraft conditions, the predicted filtered concentration is mostly dominated by graupel (51 %), cloud-ice (34 %), and snow (14 %) while there is a little contribution from supercooled rain (< 0.03 %). While in convective cloudy updrafts, cloud-ice (44 %) is the major source of ice to the predicted filtered ice concentrations, whereas large particles such as snow (34 %) and graupel (21 %) also has significant contribution and there is a very little contribution from supercooled rain (< 0.0004 %). The predicted number concentrations of snow, rain, and graupel particles (> 1 mm) conditionally averaged over these vertical velocities differ no more than 30 % from HVPS3 observations (Fig. 6l, m).

Supercooled cloud droplets and ice particles exists together in the mixed-phase region of the cloud. If supersaturation with respect to water (s_w) becomes appreciably negative, then these supercooled cloud droplets will evaporate away. The cloud becomes ice only (glaciated) once all the supercooled droplets has evaporated away and there will be no more vapour growth, riming of ice crystals and production of ice precipitation which can serve the positive feedback to ice multiplication. The theoretical ice concentration for the onset of subsaturation in the simulated storm is estimated from Korolev and Mazin 2003 (formula 22 therein). At warmer temperatures (-5 to -20^{o}C), the predicted number concentration of total ice differs by ~ 60 % (Fig. 6h) than predicted theoretical maximum of ice concentration in the cloudy convective updrafts ($w > 3$ m s^{-1}) and shows good agreement at colder temperatures (< -20^{o}C).

4.2.2 Other analysis of control simulation

As noted above (Sect. 3.1) number and mass concentrations of ice particles from various sources of ice from all primary and secondary processes were tracked using passive tagging tracers. Figure 7 shows total ice concentration from the control simulation of the storm for each species of ice represented in the AC model.

From Fig. 7c, d it can be seen that the fragmentation in ice-ice collisions is the most dominant mechanism of ice multiplication at all sub-zero temperatures both in convective updrafts and downdrafts and creates IE ratios as high as 10^3 in such updrafts and downdrafts (Fig. 7e, f). The simulated case of the MC3E had relatively warm cloud bases (-17°C) (Jensen *et al*., 2016) the HM process of rime-splintering is active at temperatures between -3 and -8°C (Fig. 7c, d). At these levels, the HM process creates IE ratios as high as 10^3 both in updraft and downdraft region (Fig. 7c, d). Upwelling carry ice splinters formed in ice multiplication mechanisms to the higher levels I the cloud. Hence, the HM process seem to be present at levels colder than -8°C. In AC, the HM process is treated with our factor multiplying the fragment emission rate (350 splinters at -5°C per mg of rime) that depends on the mean cloud droplet size. This factor is zero below 16 microns and unity above 24 microns and it is interpolated linearly in between this size range. In downdrafts, fragmentation in sublimation breakup is the second most prolific ice multiplication mechanism creating IE ratios of up to about 10^2 at temperatures colder than -10°C (Fig. 7f). Fragmentation during raindrop freezing produce less ice splinters than any other SIP processes and creates less IE ratios (~ 10) both in updraft and downdraft region.

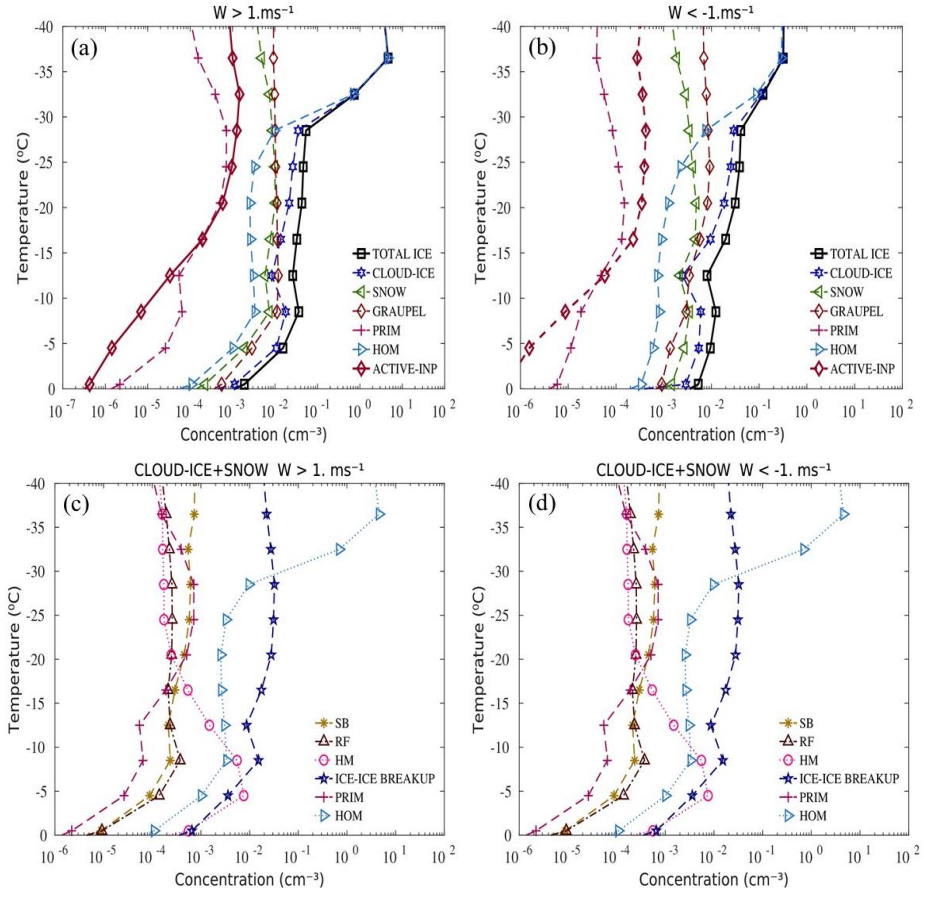

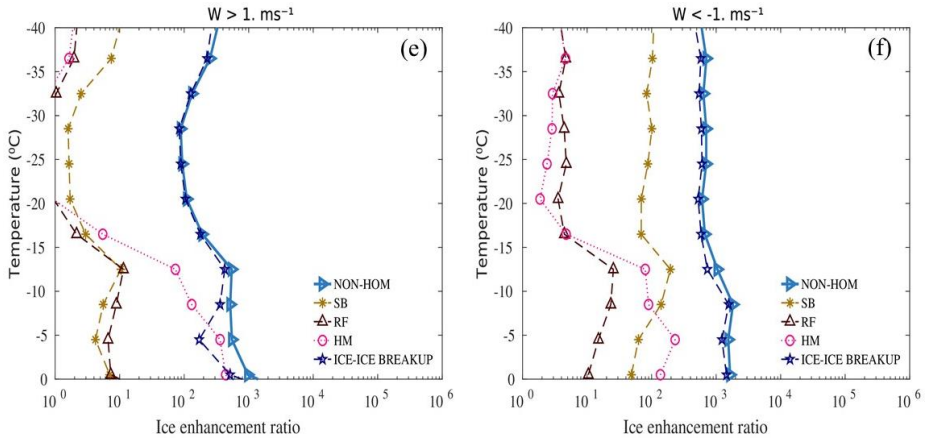

Fig. 7. Predicted number concentrations of various microphysical specious and tracer terms representing SIP processes in the AC control simulation conditionally averaged over cloudy convective updraft ($w > 1$ m s^{-1}) and downdraft ($w < -1$ m s^{-1}) conditions. (a, b) Predicted number concentration of active INP (diamond), primary ice (plus), total number concentration ice particles (solid line) and individual microphysical species (cloud-ice, snow and graupel) and total homogeneous ice (left pointing triangle), (c, d) ice concentrations (cloud-ice+snow) estimated from the tagging tracers of sublimational breakup (asterisk), fragmentation during raindrop freezing (upward pointing triangle), the HM process of rime-splintering (open circle) and fragmentation in ice-ice breakup (pentagram) conditionally averaged over these convective cloudy updrafts and downdrafts, (e, f) corresponding IE ratios from non-homogeneous ice (total cloud-ice+snow – homogeneous ice) and tracer terms of various SIP processes averaged over these vertical velocities.

Figure 8 shows a budget analysis of number of ice particles initiated by all processes represented throughout the control simulation of AC. At a first glance, it looks like fragmentation in sublimational breakup generate 500 times more ice particles than heterogenous ice at temperatures warmer than -30^{o}C. But many such fragments (80 %) formed in sublimation breakup never reach the updrafts for growth and survival (Fig. 8, black bar) and only 20 % of the fragments are survived (Fig. 8, yellow bar).

Fragmentation in ice-ice collisions generates about 100 times more particles than heterogeneous nucleation of ice at temperatures warmer than -30^{o}C (Fig. 8). Fragmentation in collisions of snow with either graupel or hail is the most prolific among all ice-ice breakup mechanisms, contributing about 46 % to the total ice from all ice-ice collisions. Also, collisions of graupel with either graupel or hail and snow on snow have appreciable impacts on the budget (~ 20 % of total fragmentation in all ice-ice collisions). Fragmentation in ice-ice collisions creates IE ratios as high as 10^2 as ice crystals formed by heterogenous freezing at warmer temperatures (> -30^{o}C) contribute only about 0.05 % to the total ice.

From Fig. 8, most of the ice particles were produced (~ 94 % of the total budget) by homogeneous freezing as cloud tops for the simulated MC3E case were well below -36^{o}C.

Compared to homogeneous freezing, various SIP mechanisms such as ice-ice breakup (3 %), the HM process (0.08 %) and raindrop freezing (0.08 %) and fragmentation in sublimation breakup (2 %) produced much less ice particles.

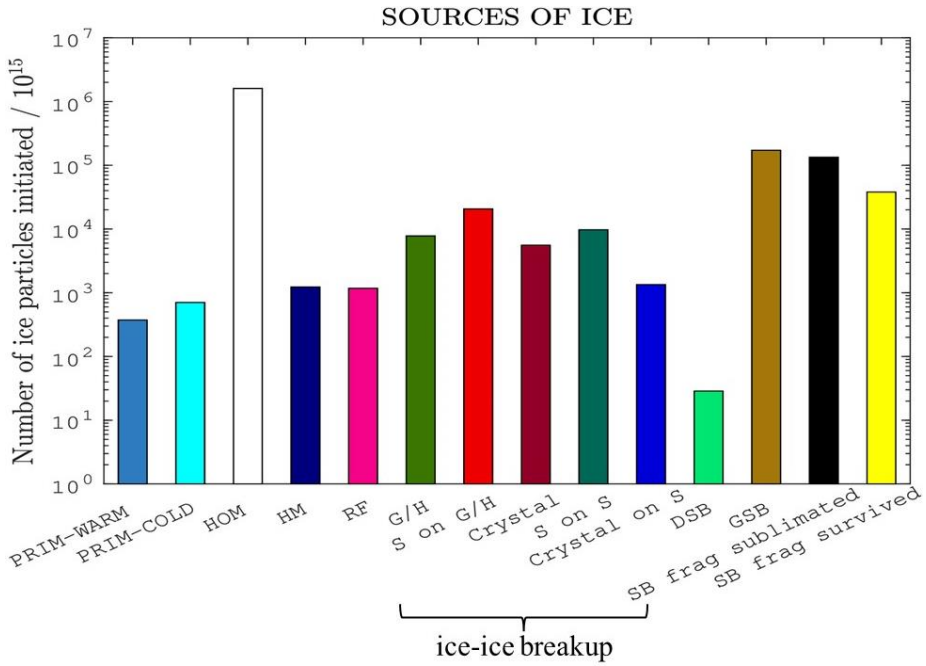

Fig. 8. Bar chart showing budgets of the number of ice crystals initiated from various processes in the control simulation of AC. (from left to right) sources of heterogeneous ice nucleation at temperatures warmer ("PRIM-WARM") and colder ("PRIM-COLD") than -30°C. Number of ice particles initiated in homogeneous freezing ("HOM") and various SIP processes such as the HM process ("HM"), fragmentation in raindrop freezing ("RF"), fragmentation in sublimational breakup of dendritic crystals/snow ("DSB") and graupel (GSB). Number of ice particles initiated in various types of breakup in ice-ice collisions such as collisions of graupel with either graupel or hail ("G/H"), snow on either snow ("S on S") or graupel or hail ("S on G/H"), crystal-crystal collisions ("Crystal"), crystal-snow collision ("Crystal on S"). Number of sublimationally generated particles that are sublimated away while descending ("SB frag sublimated") and number of sublimationally generated particles that are survived and can reach the updrafts ("SB frag survived").

4.3 Cloud-top temperature dependency of SIP

Hobbs *et al*. (1980) sampled developing cumulus clouds in the vicinity of Miles City, Montana, USA at levels warmer (by 2 and 17 K) than the instantaneous cloud tops. They used the planetary boundary layer measurements of active INP by assuming cloud-top temperature as temperature of activation. And a classic plot of IE ratio as a function of cloud-top temperature were plotted (Hobbs *et al*. 1980, Fig. 25 therein). Hobbs *et al*. (1980) observed a peak in IE ratio at cloud-top temperatures near -12°C level.

We have inferred a similar relation from the AC control simulation to analyze the cause of that classic plot, partly using tagging tracers noted above (Sect. 3.1). For the simulated MC3E case, cloud tops were detected using method described in section 4.1. Figure 9a shows predicted number concentrations of active INP (prognostic scalars from the empirical parameterization) and ice particles plotted against temperatures of coincident cloud tops. To avoid any ice from homogeneous freezing, only cloud tops warmer than -30^{o}C were selected in the analysis. It is estimated that the average ages of the clouds sampled in the present study were typically lies between 5 to 30 mins. To estimate the IE ratio, coincident number concentrations of active INP and ice were taken from the first level below the cloud-top (1 to 5 K warmer), where both were non-zero and the corresponding profile of ice enhancement ratio is shown in Fig. 9b.

The predicted IE ratio shows a peak (10^3) at -11^{o}C cloud-top temperature which is similar to the observed peak (Hobbs *et al*. 1980). This peak is predicted to arise from the HM process of rime-splintering but partly also from fragmentation in ice-ice breakup. It is predicted that splinters formed in the HM process tend to accumulate near the -11^{o}C due to increased stability of the atmosphere above this level. As any typical cloud (e.g., cumulus congestus) grow further towards its mature stage with its tops reaching well above the -16^{o}C, ice multiplication is mostly due to fragmentation in ice-ice collisions.

The HM process is predicted to prevail in the overall ice multiplication in young convective clouds with ascending tops between -7 and -11^{o}C and creates IE ratios as high as 10^3. Also, fragmentation in ice-ice collisions is predicted to create similar orders of magnitude of IE ratios at these temperatures. The HM process can prevail in clouds that are younger with warmer tops as it is inherently faster than fragmentation in ice-ice collisions (Yano and Phillips, Fig. 4 therein). The HM process is proportional to the total riming rate of graupel whereas fragmentation in ice-ice collisions is slower yet eventually more powerful ice multiplication mechanism, with its positive feedback between riming of snow to become graupel, snow-graupel collisions and growth of fragments to become snow (Yano and Phillips, 2011; Phillips *et al*., 2017b). This difference in natural time scales of the explosive growth of concentrations among these SIP mechanisms explains why studies by aircraft of warm-topped (warmer than -30^{o}C) ascending turrets have frequently reported strong correlations of observed concentrations

of ice with the HM process (Hallett *et al.*, 1978; Harris-Hobbs and Cooper 1987; Blyth *et al.*, 1997).

The HM process and fragmentation in ice-ice collisions can be ranked as the first and second most prolific mechanisms of ice multiplication in young, developing cumulus clouds. And splintering in freezing rain or drizzle and sublimation breakup can be ranked as third and fourth most prolific ice multiplication mechanism creating IE ratios of about 10^2 and 10 at temperatures between -7 and -11°C. The predicted IE ratio decrease with increasing cloud tops and increase with increasing the speed of ascent.

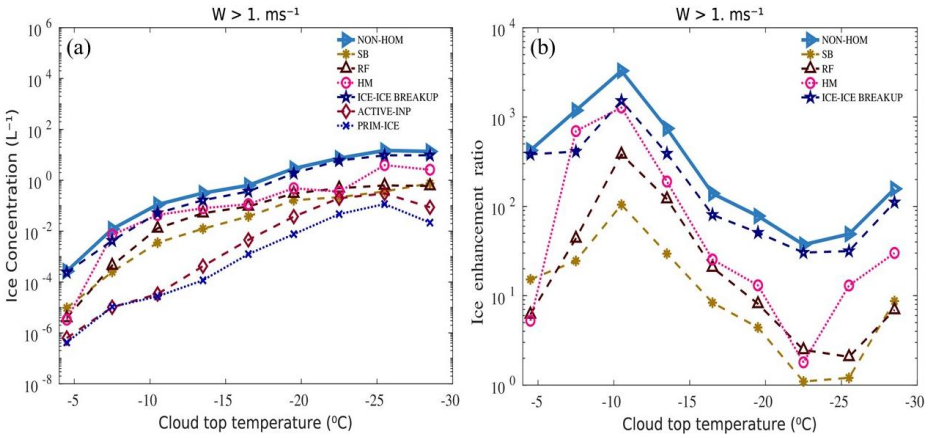

FIG. 9. (a) Predicted number concentrations of active INP (diamond), primary ice (cross), total non-homogeneous ice (right pointing triangle) and ice from various SIP mechanisms such as sublimation breakup (asterisk), shattering of freezing rain/drizzle (upward pointing triangle), the HM process (open circle) and fragmentation in ice-ice collisions (pentagram). (b) IE ratios derived from (a).

4.3.1 Schematic cloud structure

Figure 10 shows a schematic structure of growing cloud (derived from Sect. 4.1) from the control simulation of the MC3E. The temperature of cloud base is 15°C and cloud-top grows from -5 to -50°C in 60 mins. Ice multiplication is absent in typically young clouds with top near -5°C. Ice multiplication is mostly due to the HM process as cloud grows further in time (10-15 mins), with its tops reaching up to -15°C level while other SIP mechanisms contribute less to the total ice in such clouds. When cloud top reach above -30°C, along with the HM

process, other ice multiplication mechanisms also become active than they were before. Amongst which breakup in ice-ice collisions is the most dominant at all sub-zero temperatures throughout the cloud structure and contribute more than 90 % to the total ice formed at temperatures colder than -15°C level.

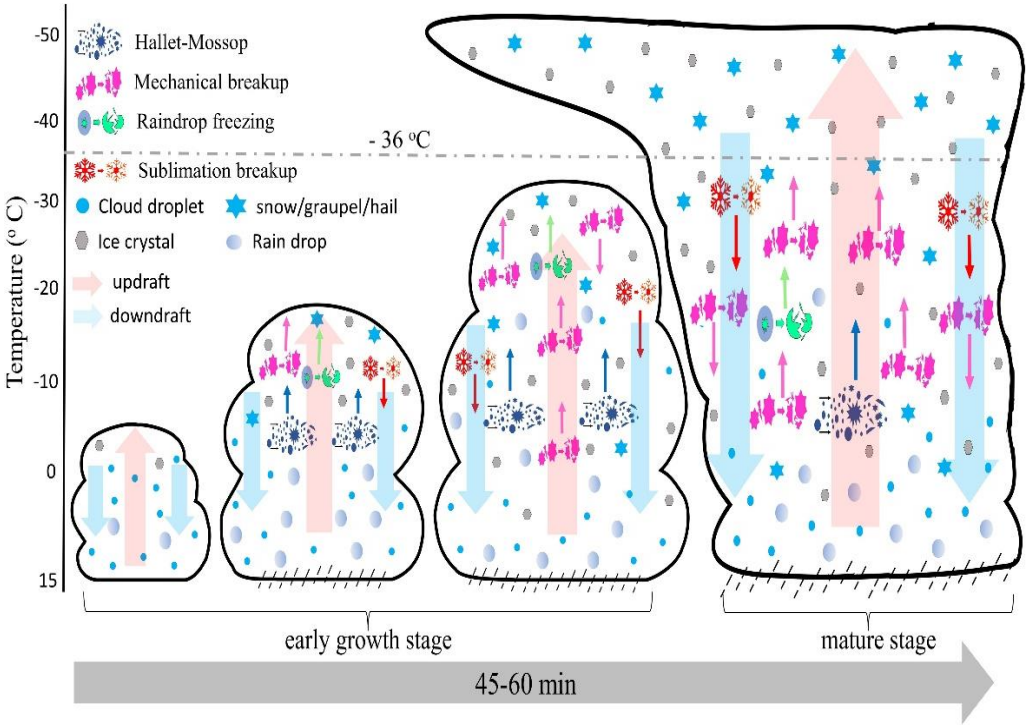

FIG. 10. The schematic cloud structure in MC3E with cloud base at 15°C and tops growing from -5 to -50°C from the control simulation showing various SIP processes active. Upwelling (downwelling) of splinters formed in such SIP processes is indicated by small upward (downward) arrows on its top (bottom). The large arrow at the bottom indicates the typical timescale of the cloud.

5. Methodology for future objectives (objectives 2-5)

5.1 ACAPEX

Atmospheric rivers (AR, narrow bands of enhanced water vapour associated with the warm sector of extratropical cyclones over the Pacific and Atlantic oceans) and aerosols are crucial elements in predicting precipitation variability (Leung, 2016). During the winter, the western US receives precipitation when storms approach from the Pacific Ocean. The department of energy (DOE) Atmospheric Radiation Measurement (ARM) Cloud-Aerosol-Precipitation Experiment (ACAPEX) was carried out in 2015 between January 15 to March 8. ACAPEX focused on following objectives:

- How do aerosols (from local pollutants and long-range transport) affect the phase and amount of precipitation?
- How frequent are aerosols transported across the Pacific? What characteristics of aerosols make them effective CCN and/or INP?

ACAPEX included four aircrafts for various measurements (such as ice particle concentrations, LWC, cloud droplet properties, etc). These were DOE G-1, National Oceanic and Atmospheric Administration (NOAA) G-IV, P-3, and NASA ER-2). The campaign also had NOAA research ship, carrying on board ARM mobile facility 2 (AMF2) which provided critical measurements to quantify the cloud and precipitation processes and moisture budget associated with ARs.

6. Progress Report

6.1 Research Plan

As a part of the research plan, total three main objectives have been proposed. The manuscript 1 based on objective 1 has been accepted for publication in the Journal of the Atmospheric Sciecnes (JAS) while second manuscript is submitted in the same journal.

Table 2. *Proposed research plan*

Year/Semester	Completed/Planned work	Completed/Planned Course credits (60 total)
Oct. 2019 - Oct. 2020 (First year)	• Simulated MC3E case in the AC model • Validated the simulated MC3E case with aircraft, satellite, and ground-based observations • Performed various sensitivity tests for the simulated MC3E case	13.5
Nov. 2020 - Oct. 2021 (Second year)	• Development of cloud-top detection algorithm to identify cloud-top temperatures for the simulated case • Studying cloud-top dependency of ice enhancement ratio and ranking the SIP mechanisms according to their order of importance in deep convective clouds • 18th ICCP conference (Aug 2021) • Submitted the research article on ice enhancement ratio	5.0
Nov. 2021 – Oct. 2022 (Third year)	• Problem analysis report and first year seminar • Revision of the previously submitted research article • Formulation of time-dependence freezing of ice nuclei • Mid-way seminar • Submission of a research article • AMS-Collective Madison Meeting, USA (Aug. 2022)	30.5
Nov. 2022 – Oct. 2023 (Fourth year)	• Thesis writing and revision of submitted research articles • AGU-December 2022 • EGU-Apr/May 2023	-

	• Thesis (feedback and correction) • PhD defence (September 2023)	

797

798 **6.2 Course work**

799 I am currently holding 49 credits out of the required 60 (Table 3), with addition
800 of 8 from the first-year seminar, the total will be 57. The plan to secure remaining
801 credits include credit awarding activities such as poster/oral presentation in
802 conferences and mid-way seminar. The mid-way seminar is planned for February
803 2023.

804

805 ***Table 3.*** Completed courses and credit details

Course	**Credits**
General Introductory Course for PhD Students (NAMN001)	0.5
Introduction for PhD students at CGB	3
Modelling project (Part of NGEN13)	5
Dynamic meteorology 2 (NGEA25)	2
Synoptic meteorology (NGEA17)	3.5
General Physical Geography (NAGE006)	4.5
Global Elemental Cycles and Environmental Change	3
Statistics for Biologists	7.5
Written English for Scholarly Publications	5
Scientific Computing with Python and Fortran	7.5
Computational Programming with Python	7.5
Total	**49 (+8) = 57**

806

807 **6.3 Progress on each objective/paper**

808

1. **Dependency of four mechanisms of secondary ice production on cloud top temperature in a continental convective storm.**
(**Waman, D.**, Patade, S., Jadav, A., Deshmukh, A., Gupta, A., Phillips, V. T. J., Bansemer, A., DeMott, P.)
Progress- This paper has been accepted for publication in the Journal of the atmospheric sciences (JAS) and is now under production.

2. **Effect from time dependence of ice nuclei activation for contrasting cloud types.**
(**Waman, D.**, Deshmukh, A., Jadav, A., Patade, S., Gautam, M., Phillips, V. T. J., Bansemer, A., Jakobsson, J., Kristensen, T.)
Progress- Literature survey, data collection, model and observational data analysis is completed. Manuscript is submitted to the JAS.

3. **The influence of multiple groups of biological ice nucleating particles on microphysical properties of mixed-phase clouds observed during MC3E.**
(Patade, S., **Waman, D.**, Deshmukh, A., Gupta, A.K., Jadav, Phillips, V., A., Bansemer, A., Carlin, J. and Ryzhkov, A.)
Progress and contribution- This study is now published in the Atmospheric Chemistry and Physics (ACP, 2022). In the present study, I was actively participated in creating the required sounding and forcing data to simulate a case of convective storm, analysing aircraft data and in model development.

4. **Time dependence of heterogeneous ice nucleation by ambient aerosols: laboratory observations and a formulation for models.**
(Jakobsson, J., **Waman, D. B.**, Phillips, V. T. J., Bjerring Kristensen, T.)
Progress and contribution-s This paper is recently published in the ACP. I have performed statistical tests on the laboratory data to test the uniqueness of various aerosol groups.

Acknowledgements

The project was funded mainly through a research grant to Vaughan Phillips (VTJP) from the Swedish Research Council for Sustainable Development ('FORMAS' Award 2018-01795). Dr. Sachin Patade was actively participated in model development and aircraft data analysis. Arti Jadav created codes to estimate the forcing from radiosonde and which was prerequisite for setting up the model and for analysis of observational data.

Appendix

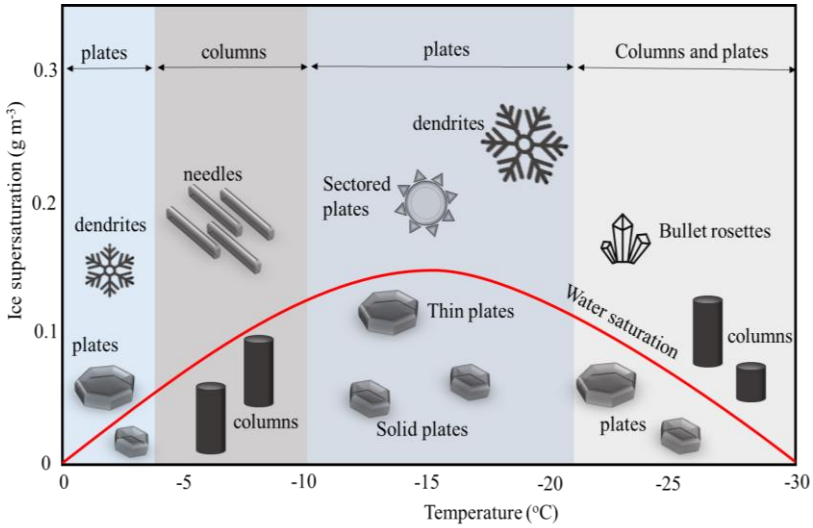

Fig. A1. Ice particle morphology illustrating habits of ice crystals as a function of ice supersaturation and ambient temperature.

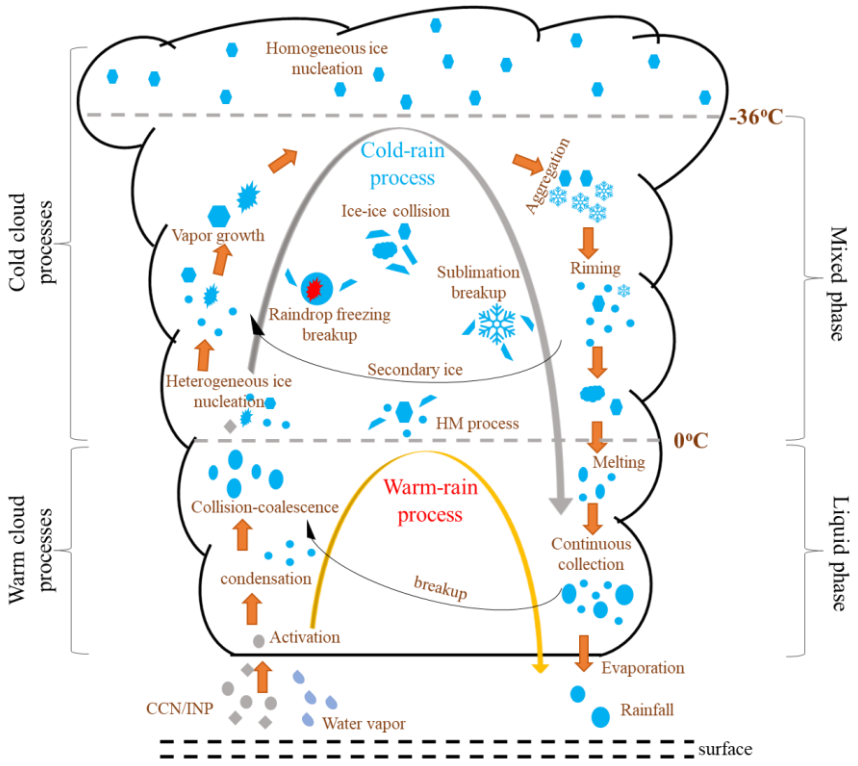

Fig. A2. Schematic structure of cloud with top reaching up to the level of tropopause. Various processes of warm and cold cloud microphysics including secondary ice production mechanisms active that are discussed in Sec. 2 shown.

References

Auer, A. H., D. L., Veal, and J. D., Marwitz, 1969: Observations of ice crystal and ice nuclei concentrations in stable cap clouds. *J. Atmos. Sci.*, **26**, 1342–1343.

Bacon, N. J., B. D., Swanson, M. B., Baker, and E. J., Davis, 1998: Breakup of levitated frost particles. *J. Geophys. Res.*, **103**, 13763–13775.

Beard, K. V., 1992: Ice initiation in warm-base convective clouds: An assessment of microphysical mechanisms. *Atmos. Res.*, **28**, 125–152.

Blyth, A. M. and J., Latham, 1993: Development of ice and precipitation in New Mexican summertime cumulus clouds. *Quart. J. Roy. Meteorol. Soc.*, **119**: 91-120.

Blyth, A. M., R. E., Benestad, P. R., Krehbiel, 1997: Observations of supercooled raindrops in new Mexico Summertime Cumuli. *J. Atmos. Sci.*, **54**, 569-575.

Cantrell, W., and A., Heymsfield, 2005: Production of ice in tropospheric clouds: A review. Bulletin of the American Meteorological Society, **86(6)**, 795–807.

Chin, M., R. B., Rood, S. J., Lin, J. F., Müller, and A. M., Thompson, 2000: Atmospheric sulfur cycle simulated in the global model GOCART: Model description and global properties. *J. Geo. Res.*, **105(D20)**, 24671–24687.

DeMott, P. J., D. J., Cziczo, A. J., Prenni, D. M., Murphy, S. M., Kreidenweis, D. S., Thomson, R., Borys, and D. C., Rogers, 2003: Measurements of the concentration and composition of nuclei for cirrus formation. *P. Natl. Acad. Sci. USA*, **100(25)**, 14655–14660.

DeMott, P.J., O., Möhler, O., Stetzer, G., Vali, Z., Levin, M. D., Petters, M., Murakami, T., Leisner, U., Bundke, H., Klein, Z. A., Kanji, R., Cotton, H., Jones, S., Benz, M., Brinkmann, D., Rzesanke, H., Saathoff, M., Nicolet, A., Saito, B., Nillios, H., Bingemer, J., Abbatt, K., Ardon, E., Ganor, D. G., Geogakopoulos, and C., Saunders, 2011: Resurgence in ice nuclei measurement research. *B. Am. Meteorol. Soc.*, **92**, 1623–1635.

DeMott, P. J., A. J., Prenni, G. R., McMeeking, R. C., Sullivan, M. D. Petters, Y. Tobo, M. Niemand, O. Möhler, J. R. Snider, Z. Wang and M. Kreidenweis, 2015: Integrating laboratory and field data to quantify the immersion freezing ice nucleation activity of mineral dust particles. *Atmos. Chem. Phys.*, **15**, 393-409. doi:10.5194/acp-15-393-2015.

Deshmukh, A., V. T. J. Phillips, A. Bansemer, S. Patade, D. Waman, 2021: New empirical formulation for the sublimational breakup of graupel and dendritic snow. *J. Atoms. Sci.*, https://doi.org/10.1175/JAS-D-20-0275.1

Field, P. R., Heymsfield, A. J., and Bansemer, A., 2006: Shattering and particle interarrival times measured by optical array probes in ice clouds. *J.Atmos. Ocean. Tech.*, **23(10)**, 1357–1371.

Field, P. R., A. J., Heymsfield, 2015: Importance of snow to global precipitation. *Geo. Phys. Res. Lett.*, **42**, 9512-9520.

Field, P. R., R. P., Lawson, P. R. A., Brown, G., Lloyd, C., Westbrook, D., Moisseev, A., Miltenberger, A., Nenes, A., Blyth, T., Choularton, P., Connolly, J., Buehl, J., Crosier, Z., Cui, C., Dearden, P., DeMott, A., Flossmann, A., Heymsfield, Y., Huang, H., Kalesse, Z. A., Kanji, A., Korolev, A., Kirchgaessner, S., Lasher-Trapp, T., Leisner, G., McFarquhar,

V., Phillips, J., Stith, S., Sullivan, 2017: Secondary ice production: Current state of the science and recommendations for the future. Ice Formation and Evolution in Clouds and Precipitation: Measurement and Modeling Challenges, Meteor. Monogr., No. **58**, *Amer. Meteor.Soc.*,7.1-7.20, https://journals.ametsoc.org/doi/pdf/10.1175/AMSMONOGRAPHS-D-16-0014.1.

Fridlind, A. M., A. S., Ackerman, G., McFarquhar, G., Zhang, M. R., Poellot, P. J., DeMott, A. J., Prenni, and A. J., Heymsfield, 2007: Ice properties of single-layer stratocumulus during the Mixed-Phase Arctic Cloud Experiment: 2. Model results, *J. Geophy. Res.*, **112(24)**, 1–25.

Hallett, J., and S. C., Mossop, 1974: Production of secondary ice par- ticles during the riming process. *Nature*, **249**, 26–28.

Harris-Hobbs, R. L., and W. A., Cooper, 1987: Field evidence supporting quantitative predictions of secondary ice pro- duction rates. *J. Atmos. Sci.*, **44**, 1071–1082.

Hobbs, P. V., 1971: Studies of winter cyclonic storms over the Cascade Mountains (1970–71). Research Rep. VI, Dept. of Atmospheric Sciences, University of Washington, 306 pp.

Hobbs, P. V., and R., Farber, 1972: Fragmentation of ice particles in clouds. *J. Rech. Atmos.*, **6**, 245-258.

Hobbs, P. V., S., Chang and J. D., Locatelli, 1974: The dimensions and aggregation of ice crystals in natural clouds. *J. Geo. Res.*, **79**.

Hobbs, P. V., M. K. Politovich, and L. F. Radke, 1980: The structures of summer convective clouds in eastern Montana. I: Natural clouds. *J. Appl. Meteor.*, **19**, 645–663.

Hobbs, P. V., 1969: Ice multiplication in clouds, *J. Atmos. Sci.*, **26**, 315–318.

Jensen, M. P., Petersen, W. A., Bansemer, A., Bharadwaj, N., Carey, L. D., Cecil, D. J., Collis, S. M., Del Genio, A. D., Dolan, B., Gerlach, J., Giangrande, S. E., Heymsfield, A., Heymsfield, G., Kollias, P., Lang, T. J., Nesbitt, S. W., Neumann, A., Poellot, M., Rutledge, S. A., Schwaller, M., Tokay, A.,Williams, C. R.,Wolff, D. B., Xie, S., and Zipser, E. J., 2016: The Midlatitude Continental Convective Clouds Experiment (MC3E), *B. Am. Meteorol. Soc.*, **97**, 1667–1686.

King, W. D., and N. H. Fletcher, 1973: Pressures and stresses in freezing water drops. *J. Phys.*, **6D**, 2157-2173.

Korolev, A., I. P. Mazin, 2003: Supersaturation of water vapor in clouds. *J. Atmos. Sci.*, **60**, 2957-2974.

Korolev, A. V., E. F., Emery, J. W., Strapp, S. G., Cober, G. A., Isaac, M., Wasey, and D., Marcotte, 2011: Small ice particles in tropospheric clouds: Fact or artifact? Airborne icing instrumentation evaluation experiment, *B. Am. Meteorol. Soc.*, **92(8)**, 967–973.

Kuan-Man-Xu., 1994: Partitioning Mass, Heat and Moisture Budgets of Explicitly Simulated Cumulus Ensembles into Convective and stratiform Components. *J. Atmos. Sci.*, **52**, doi.org/10.1175/1520-0469(1995)052<0551:pmhamb>2.0.CO;2.

Leisner, L., T., Pander, P., Handmann, and A., Kiselev, 2014: Secondary ice processes upon heterogeneous freezing of cloud droplets, 14th Conf. on Cloud Physics and Atmospheric Radiation, Boston, MA, *Amer. Meteor. Soc.*, 2.3, https://ams.confex. com/ams/14cloud14atrad/webprogram/Paper250221. html.

Leung, L. R., 2016: ARM Cloud-Aerosol-Precipitation Experiment (ACAPEX) field campaign report, DOE/SC-ARM-16-012.

Mossop S. C. and A., Ono, 1969: Measurements of Ice Crystal Concentration in Clouds, *J. Atmos. Sci.*, **26**, 99-117.

Mossop S. C., and J., Hallett, 1974: Ice crystal concentration in cumulus clouds: influence of the drop spectrum. Science, **186**,632-634.

Mossop S. C., 1976: Production od secondary ice particles during the growth of graupel by riming. *Quart. R. Meteor. Soc.*, **102**, 45-57.

Oraltay, R. G. and J., Hallett, 1989: Evaporation and melting of ice crystals: A laboratory study, *Atmos. Res.*, **24**, 169–189.

Patade, S., V. T. J., Phillips, P., Amato, H. G., Bingemer, S. M., Burrows, P. J., DeMott, P. J., Goncalves, F. L. T., Knopf, D. A. Morris, C. E., Alwmark, C., Artaxo, P., Pöhlker, C., Schrod, J., B., Weber, 2021: Empirical formulation for multiple groups of primary biological ice nucleating particles from field observations over Amazonia. *J. Atmos. Sci.*, **78(7)**, 2195-2220.

Phillips, V. T. J., A. M., Blyth, T. W., Choularton, P. R. A., Brown, J., Latham, 2001: The glaciation of a cumulus cloud over New Mexico. *Quart. J. Roy. Meteor. Soc.*, **127**, 1513-1534.

Phillips, V. T. J. P., P. J., DeMott, and C., Andronache, 2008: An empirical parameterization of heterogeneous ice nucleation for multiple chemical species of aerosol. *J. Atmos. Sci.*, **65**, 2757-2738.

Phillips, V. T. J., J. I., Yano, A., Khain, 2017: Ice multiplication by breakup in ice-ice collisions. Part I: Theoretical formulation, *J. Atmos. Sci.*, **74(6)**, 1705–1719.

Phillips, V. T. J., J. I., Yano, M., Formenton, E., Ilotoviz, V. P., Kanawade, I., Kudzotsa, J., Sun, A., Bansemer, A. G., Detwiler, A., Khain, S. A., Tessendorf, 2017: Ice multiplication by breakup in ice-ice collisions. Part II: Numerical simulations, *J. Atmos. Sci.*, **74(9)**, 2789–2811.

Phillips, V. T. J., S. Patade, J., Gutierrez, A., Bansemer, 2018: Secondary ice production by fragmentation of freezing drops: Formulation and theory, *J. Atmos. Sci.*, **75(9)**, 3031–3070.

Phillips, V. T. J., M., Formenton, V. P., Kanawade, L. R., Karlsson, S. Patade, J., Sun, C., Barthe, J. P., Pinty, A. G., Detwiler, W., Lyu, S. A., Tessendorf, 2020: Multiple environmental influences on the lightning of cold-based continental cumulonimbus clouds. Part I: Description and validation of model, *J. Atmos. Sci.*, **77(12)**, 3999–4024.

Pruppacher, H., and R. J. Schlamp, 1975: A wind tunnel investigation on ice multiplication by freezing of waterdrops faling at terminal velocity in air. *J. Geophys. Res.*, **80**, 380-386.

Pruppacher, H., and J., Klett, 1997: Microphysics of Clouds and Precipitation. 2nd ed. Atmospheric and Oceanographic Sciences Library, Vol. **18**, Kluwer Academic Publishers, 954 pp.

Radke, L. F., and P. V. Hobbs, 1969: Measurements of cloud condensation nuclei, light scattering coefficient, sodium containing particles and Aitken nuclei in the Olympic Mountains of Washington. *J. Atmos. Sci*, **26**, 281-288.

Rogers, R. R., and M. K., Yau, 1989: A short Course in Cloud Physics. 3rd ed. International Series in Natural Philosophy, Butterworth-Heinemann, 304 pp.

Schaefer, V. J., and R. J. Cheng, 1971: The production of ice crystal fragments by sublimation and electrification. *J. Rech. Atmos.*, **5**, 5-10.

Takahashi, T., Y., Nagao, Y., Kushiyama, 1995: Possible high ice particle production during graupel–graupel collisions, *J. Atmos. Sci.*, **52**, 4523–4527.

Tao, W. K., and J., Simpson, 1989: Modeling study of a tropical squall-type convective line. *J. Atmos. Sci.*, **46**, 177-202.

Vardiman, L., 1978: The generation of secondary ice particles in clouds by crystal–crystal collision, *J. Atmos. Sci.*, **35**, 2168–2180.

Yano, J.I. and V. T. J., Phillips, 2011: Ice–Ice Collisions: An Ice Multiplication Process in Atmospheric Clouds, *J. Atmos. Sci.*, **68**, 322–333.

Wallace, J. M., and Hobbs, P. V., (1977) Atmospheric science, an introductory survey, Academic press, New York, 46/pp.

Glossary

CIP: Cloud-Imaging Probes (25 µm – 1500 µm).

2DC: 2D cloud imaging probe (30 µm – 1000 µm).

HVPS-3: High-volume precipitation spectrometer version 3 (150 µm – 19200 µm).

Vapor pressure: Pressure exerted over the liquid by its vapor molecules.

Saturation vapor pressure: Pressure exerted over the liquid by its vapor molecules in equilibrium.

Condensation: An exothermic process in which vapor molecules transform into liquid molecules

Evaporation: An endothermic process in which liquid molecules transform into vapor molecules.

Sublimation: An endothermic process in which solid phase of an element is directly transform into the vapor phase.

Mixing-ratio: The mass of water vapor per unit mass of dry air is known as the mixing ratio. It can be expressed in g/kg.

Saturation mixing ratio: Mixing ratio of saturated air.

Relative humidity: Ratio of actual mixing ratio to the saturation mixing ratio.

Supersaturation: Condition in which relative humidity is greater than 100 % and can be defined as RH-100 %.

Cloud Condensation Nuclei (CCN): Suspended hygroscopic particles in the atmosphere which can serve as centres for condensation are known as CCN.

Ice Nuclei (IN): Suspended solid particles in the atmosphere which can acts as the nucleus for the formation of ice crystal.

Homogeneous nucleation: The process of formation of pure cloud droplets (or ice crystals) by condensation from a supersaturated vapor without the aid of foreign particles CCN (or IN in case of ice) is known as homogeneous nucleation. It occurs at temperatures colder than -36^{o} C.

Heterogeneous nucleation: The process of formation cloud droplets (or ice particles) by condensation of supersaturated vapor on CCN (or IN in case of ice) is known as heterogeneous nucleation. Heterogeneous nucleation can occur at temperatures warmer than -36^{o} C.

Cloud-droplets: Condensational product of water vapor are known as cloud droplets. The approximate size of cloud droplet is 1-100 µm in diameter.

Supercooled cloud droplets: Cloud droplets that remain liquid at temperatures below 0^{o} C.

Cloud-ice crystals: Ice particles formed by vapor diffusional growth under various conditions of temperature and humidity. Ice particles can be found in wide variety of shapes (e.g., dendrites, needles, columns, plates, etc)

Coalescence: Process in which smaller cloud droplets collide and overtake by the larger cloud drops. Collision efficiency is negligible if both droplets are smaller than 10-20 µm and collision cannot occur.

Collision efficiency: The probability of collision of two drops if one is in the path swept out by the other is known as collision efficiency.

Warm rain process: It includes growth of cloud droplet by collision-coalescence.

Liquid water content (LWC): Amount of liquid water present in unit volume of air (g m^{-3}).

Cloud droplet concentration: Total number of cloud droplets present in unit volume of air (#/cm^{-3}).

Vapor-diffusional growth: In the mixed phase cloud where supercooled cloud droplets and ice crystals co-exist, the air is saturated with respect to liquid water and hence supersaturated with respect to ice. In such environment, ice particles will grow more rapidly from vapor phase than droplets. This process is known as vapor diffusion.

Accretion: Process in which supercooled cloud droplet is captured by an ice phase precipitating particle. Riming is the accretion process in which droplet freeze immediately on contact with an ice particle forming a coating of rime leading to formation of rimed crystal or graupel.

Riming: In mixed phase cloud where supercooled cloud droplets and ice crystals can co-exist. Ice particles can increase in mass by colliding with these supercooled cloud droplets that later

freeze onto them. This process is known as riming. If the freezing is not immediate, denser structures are created of which hail is an extreme example.

Aggregation: Process of formation of snowflakes by clumping of ice crystals.

Rain: Type of precipitation that forms because of collision-coalescence of cloud-droplets.

Raindrop: Liquid particles in the form of precipitation. Typical size of raindrop is 0.1 to 5 mm.

Primary ice: Ice particle formed only by heterogeneous or homogeneous nucleation and not by any other mechanism is known as primary ice.

Secondary ice: Ice particle formed by processes other than heterogeneous or homogeneous nucleation. It typically involves fragmentation of pre-existing ice particles.

Snow: Product of aggregation composed of ice crystals. Snow is not heavily rimed.